ROLE OF AN ORGANIC MEDIUM IN THE FORMATION OF Au, Fe, AND AuFe NANOPARTICLES OBTAINED BY METAL VAPOR SYNTHESIS

A. A. Voronova, A. V. Naumkin, and A. Yu. Vasil'kov*

Nesmeyanov Institute of Organoelement Compounds, Russian Academy of Sciences, ul. Vavilova 28, str. 1, Moscow, 119334 Russia

Cite this: *INEOS OPEN*, **2022**, *5 (3)*, 79–84
DOI: 10.32931/io2215a

Received 3 February 2023,
Accepted 2 March 2023

http://ineosopen.org

Abstract

Nanomaterials based on Au, Fe, and AuFe are obtained by metal vapor synthesis using acetone as a dispersion medium. The comparative analysis by X-ray photoelectron spectroscopy (XPS), energy dispersive X-ray spectroscopy (EDX), and scanning electron microscopy (SEM) reveals a significant amount of the fragments of organic compounds on the surface of the resulting nanoparticles. The Au and Fe nanoparticles display antibacterial activity against *Escherichia coli* and *Bacillus cereus*.

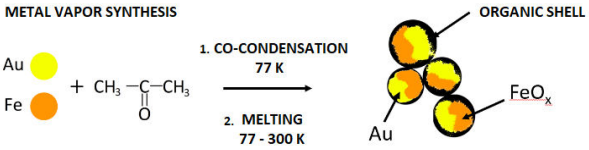

Key words: nanoparticles, metal vapor synthesis, X-ray photoelectron spectroscopy, energy dispersive X-ray spectroscopy.

Introduction

Today cancer is the leading cause of morbidity and mortality in the world and represents a serious challenge for public health services [1]. Chemotherapy plays an important role among different effective means of combating oncological diseases. However, affecting primarily rapidly dividing cells, it can have a toxic effect on both cancerous and healthy cells, including the cells of bone marrow and digestive tract, macrophages, *etc.* [2].

The problems associated with the conventional chemotherapy can be solved, in particular, by the application of metal nanoparticles which have already proved efficient in cancer treatment owing to selectivity and a possibility to serve as drug carriers [3, 4]. The investigations performed in the recent decades demonstrated that the size, morphology, and properties of metal nanoparticles strongly depend on the methods of synthesis and conditions for their formation [5–7]. The surface atoms of metal nanoparticles with unbalanced valence forces actively interact with their surrounding, which can significantly change its composition.

The use of iron oxide nanoparticles (FeO_x NPs) and gold nanoparticles (Au NPs) is stipulated by a number of peculiarities: the ability of cancer cells to selectively absorb NPs *via* nonspecific endocytosis, heat generation under the action of alternating magnetic field (magnetic hyperthermia) [8], and the possibility of application of nanoparticles for ultrasensitive detection of cancer cells [9]. Hybrid structures formed on the basis of these metal nanoparticles can improve or expand the possible applications of new composites. The systems containing Au and Fe nanoparticles are already used in catalysis [10, 11], computed tomography [12], enhanced hyperthermia [13], and other areas [14, 15]. It was shown that the introduction of gold into FeO_x NPs does not reduce the magnetization of bimetallic nanoparticles [16], which enables the use of external magnetic impact for the AuFe system as a whole [17]. Since the size, composition, and structure of these materials have a significant effect on their functional properties, the ability to control these characteristics is fundamental in any potential application. The structure and electronic state of AuFe nanoparticles change significantly depending on the method of their preparation [18, 19] and can lead to synergism [20]. This puts forward the task of developing new methods for the synthesis of AuFe systems and their comprehensive study among the priority research fields.

Ecologically friendly metal vapor synthesis (MVS) was shown to be particularly effective in this area [21–24]. This method can afford mono- and bimetallic metal nanoparticles, which significantly expands the range of available biologically active heterometallic systems. MVS allows for avoiding or significantly reducing the amount of impurities introduced into biomedical materials during their synthesis. An important advantage of this approach is the possibility of controlling the particle size and surface composition when using various organic ligands.

At the same time, the surface atoms of metal nanoparticles are extremely reactive towards their surrounding. Regardless of the metal nature, nanoparticles always have on their surface a layer of chemisorbed products of the reaction medium in which they were obtained.

It was found that, under conditions of metal vapor synthesis of metal nanoparticles using a single organic reagent, the resulting products contain a significant amount of the hydrocarbon material. As a rule, these are the fragments of the organic reagent strongly chemisorbed on the surface of the metal nanoparticles [25–27].

The presence of a hydrocarbon shell and its effect on the functional properties of the resulting materials have not been studied in detail. The situation changes when the systems

obtained are potential objects for clinical use and their diagnostics is necessary for subsequent application.

Enzymes of living biosystems are capable of processing bioorganic substances involved in the surface layer of nanoparticles. As a result, the metal surface becomes exposed. Under the action of reactive oxygen species, the nanoparticle can break down into smaller metal clusters, the reactivity of which is much higher compared to nanoparticles due to the huge contribution of surface energy. In this case, the cytotoxic objects are generated in the vicinity of the cell attacked by them. This promotes the investigation of both the composition and structure of the resulting nanoparticles and the functional properties of the systems, as well as the relationship between the properties of these systems and their structures.

The goal of this work was to synthesize monometallic gold and iron nanoparticles and bimetallic gold–iron nanoparticles by metal vapor synthesis as potential anticancer agents and to study the structures of the resulting materials and their surface compositions depending on the nature of the metal used under the MVS conditions.

Results and discussion

The iron nanoparticles obtained by MVS (Scheme 1), in contrast to the gold ones, are extremely active and are easily oxidized upon contact with air or traces of moisture and oxygen in an organic reagent. Therefore, all experiments for the preparation of mono- and bimetallic AuFe nanomaterials were performed *in situ* under vacuum or in an inert atmosphere. Varying the nature of the organic reagent, one can change both the particle size and electronic state of the metal and, as a consequence, the biological activity of the system as a whole.

The sizes and structures of the resulting nanoparticles largely depend on the organic reagent. In this work, acetone (Ac) was used as a solvent, which afforded the Au nanoparticles with the sizes of 10–30 nm [28] and the Fe nanoparticles with an average size of 2.7 nm [29].

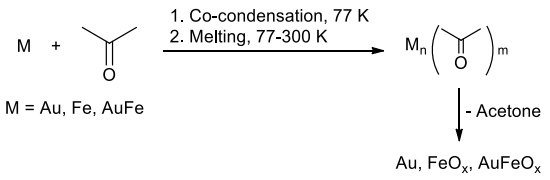

Scheme 1. Synthesis of Au, Fe, and AuFe nanoparticles using acetone as an organic medium.

According to the results of SEM analysis, the bimetallic nanoparticles condensed in an acetone matrix (AuFeAc), after the removal of the dispersion medium, form aggregates with a broad particle size distribution (Fig. 1).

The SEM micrographs of the Au–acetone (AuAc) and Fe–acetone (FeAc) systems are presented in Figs. S1 and S2 in the Electronic Supplementary Information (ESI). After the removal of acetone, the metal particles are assembled into aggregates consisting of nanoparticles, which sizes were determined by transmission electron microscopy (TEM). It was found that the average sizes of Au and Fe nanoparticles in organosols are 5.3 nm and 1.8 nm, respectively. The particle size distribution histograms are depicted in Fig. S3 in the ESI.

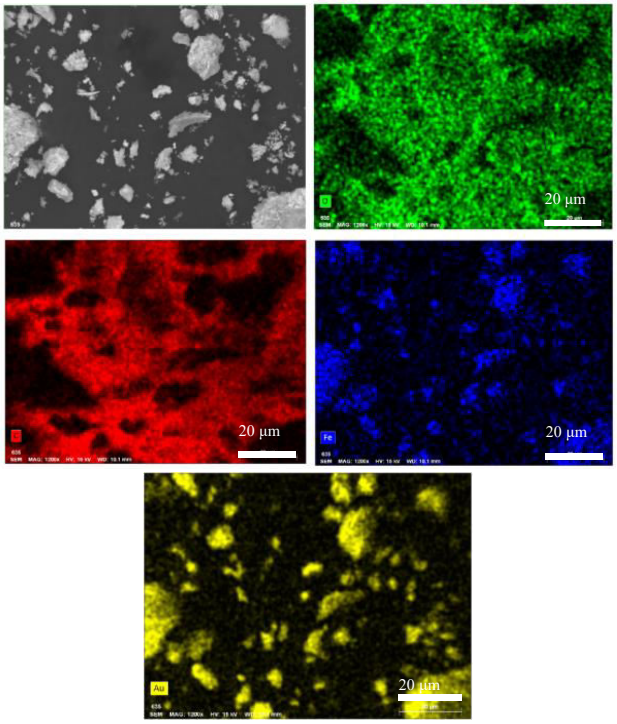

Figure 1. SEM image of the morphology and elemental maps of the AuFe black nanoparticles.

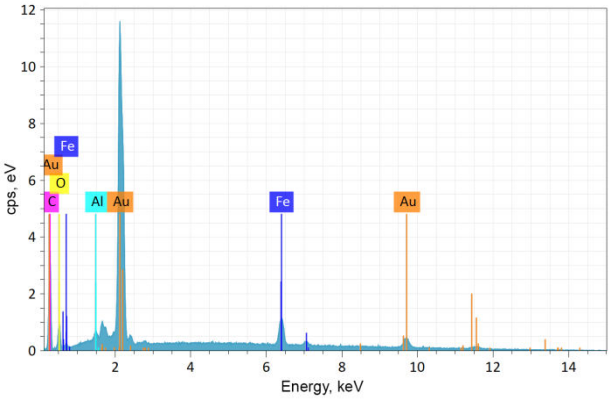

Figure 2. EDX spectrum for AuFeAc: C, 70.1 at %; O, 11.2 at %; Fe, 6.0 at %; Au, 12.6 at %.

Figure 2 shows the EDX spectrum of the AuFeAc NPs. The resulting elemental analysis data indicate that the AuFe nanoparticles differ in the reactivity from monometallic systems. A significant amount of carbon material suggests active chemisorption of acetone or its fragments on the metal surface.

Since metal nanoparticles have a high surface energy, their surface cannot remain pure and is covered with layers of the surrounding components. The high reactivity of metal clusters obtained by MVS towards hydrocarbons was demonstrated [30, 31]. The production of Au and Fe nanoparticles by MVS implies the use of vacuum and an inert atmosphere; however, their practical application is associated with exposure to air [10–15]. In this respect, the surface analysis of the freshly prepared material as well as during its subsequent storage in air is very important for understanding the composition and structure of these promising medical materials. The presence of an organic shell on the exposed surface of metal nanoparticles, which can exist only in an inert gas matrix [32, 33], is a positive factor that

allows for protecting the extremely active surface of the particle and stability of their properties.

The surface analysis was performed by XPS. The full spectra of the samples (Fig. 3) show, along with the peaks corresponding to metals, the peaks from the elements that are involved in the solvent. The elemental composition of the samples explored is presented in Table 1.

Figure 4 shows the C 1s spectra of the FeAc, AuAc, and AuFeAc samples presented as the sum of several Gaussian profiles using reference chemical shifts for the respective chemical groups. Table 2 shows the numerical characteristics of the peaks.

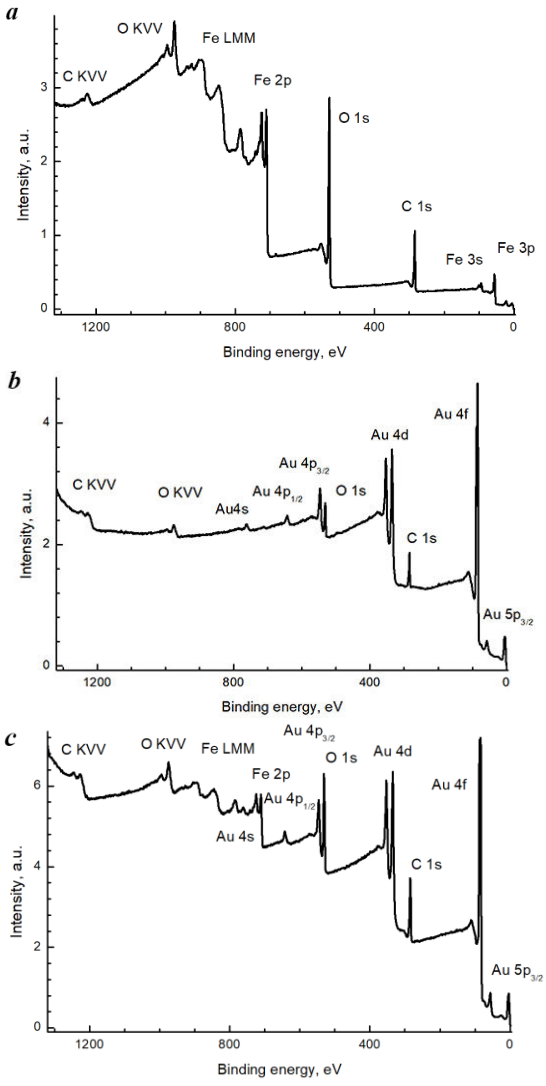

Figure 3. Full XPS spectra of the samples: FeAc (***a***), AuAc (**b**), AuFeAc (***c***).

Table 1. Concentrations of elements on the surface of the FeAc, FeAc, and AuFeAc samples (at %) calculated from the XPS spectra

Sample	Au	Fe	O	C
FeAc		29.8	35.9	34.4
AuAc	25.9		21.0	53.0
AuFeAc	12.0	14.5	25.8	47.8

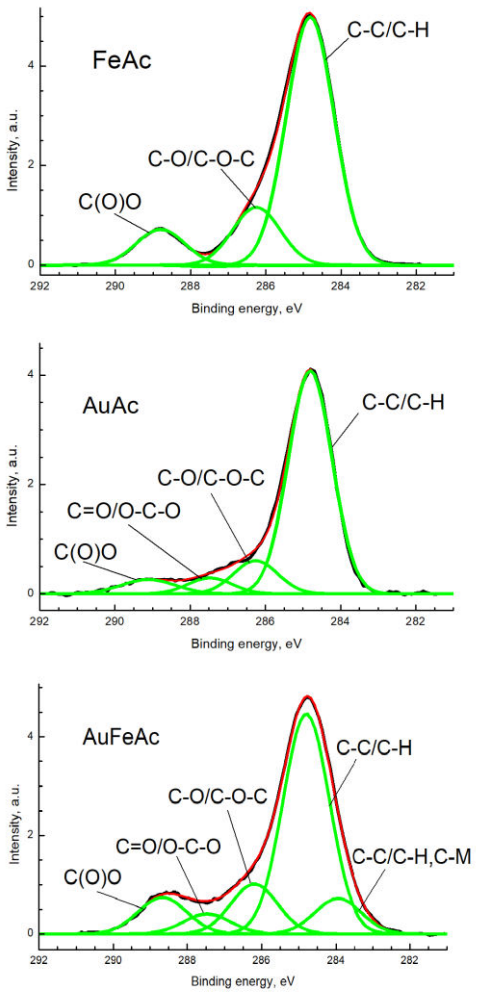

Figure 4. C 1s photoelectron spectra of the FeAc, AuAc, and AuFeAc samples.

Table 2. Characteristics of the photoelectron spectra: binding energies (E_b), widths (W), and relative intensities (I_{rel}) of the photoelectron peaks corresponding to different chemical groups in the C 1s spectra

Sample	Group	C–C/ C–H, C-M	C–C/ C–H	C–O/ C–O-C	C=O/ O–C–O	C(O)O
FeAc	E_b		285.0	286.5		289.0
	W		1.27	1.27		1.28
	I_{rel}		0.73	0.17		0.11
AuAc	E_b		285.0	286.5	287.7	289.3
	W		1.16	1.17	1.17	1.43
	I_{rel}		0.77	0.11	0.05	0.06
AuFeAc	E_b	284.1	285.0	286.4	287.7	288.9
	W	1.25	1.25	1.25	1.25	1.3
	I_{rel}	0.10	0.61	0.14	0.05	0.10

It should be noted that the chemical shifts of the C–O/C–O–C and C=O/O–C–O groups are identical in the spectra of all the samples explored, while those of the C(O)O group range within 3.9–4.3 eV. All the FeAc samples contain C–C/C–H, C–OH/C–O–C, and C(O)O groups, while the AuAc and AuFeAc samples also contain C=O/O–C–O groups.

The peak with a binding energy of 284.1 eV in the spectrum of the AuFeAc sample can be attributed to both low molecular weight C–C/C–H fragments and metal–carbon bonds [34].

Figure 5 shows the C 1s spectra of the samples under investigation, normalized by the intensity of the main peak. The data presented in Table 2 suggest that the AuFeAc sample contains the lowest amount of unoxidized carbon and the C(O)O group has the smallest chemical shift. This reflects the effect of Au and Fe atoms on the interaction with the C(O)O group and the possible appearance of bimetallic chelate complexes. Thus, the lowest binding energy of the Au $4f_{7/2}$ peak, equal to 84.0 eV, is typical, on the one hand, for large gold particles but, taking into account the size effect (ESI, Fig. S4), it can also be attributed to the Au–C bonds.

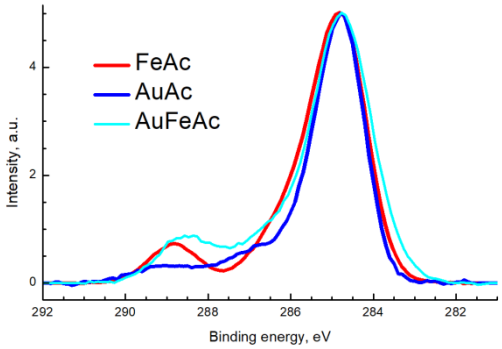

Figure 5. C 1s photoelectron spectra of the FeAc, AuAc, and AuFeAc samples normalized to the intensity of the main peak.

Figure 6a shows the O 1s spectra in which the peaks characteristic of the Fe–O bonds are well resolved but appeared to be shifted relative to each other by ~0.2 eV. This indicates the need for recalibration of the spectra of the iron-containing samples. The binding energy of the main peak in the O 1s spectrum of FeAc was found to be 530.0 eV. In this case, the considerations of the surface charge determined from the C 1s and O 1s spectra lead to the same results. To analyze the spectrum that does not contain the Fe–O state, the difference spectrum AuFeAc–FeAc was obtained, which almost coincides with the spectrum of the AuAc sample in the region of high binding energies but differs markedly from it in the region of binding energies of about 532 eV (Fig. 6b). The difference spectrum AuFeAc–FeAc–AuAc has a maximum with a binding energy close to the binding energy of the C=O and C(O*)O groups [37].

The preliminary evaluation of biological activity was carried out for the AuAc and FeAc systems. The investigation of antibacterial activity (Table 3) revealed a low bactericidal effect of AuAc against gram-negative bacteria. At the same time, FeAc exhibited higher inhibitory effects against both gram-negative *Escherichia coli* and gram-positive *Bacillus cereus*.

Table 3. Antibacterial activity of the resulting AuAc and FeAc nanoparticles

Sample	Zone of inhibition of bacterial growth (mm)	
	Escherichia coli	*Bacillus cereus*
AuAc	10 (± 0.4)	8.5 (± 0.6)
FeAc	11.75 (± 1.3)	12 (± 0.4)
Control	42 (± 1.8)	35.5 (± 1.3)

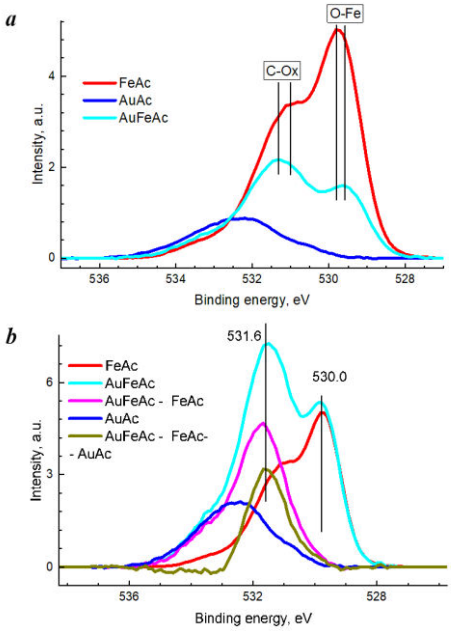

Figure 6. O 1s photoelectron spectra of the samples explored: initial sample (***a***) and sample after recalibration (***b***).

Experimental

General remarks

Acetone (Sigma-Aldrich, ACS reagent, ≥ 99.5%) was dried and distilled over zeolites under a purified argon atmosphere. Prior to the synthesis, the solvent was degassed by alternating freeze-thaw cycles. The investigations were concerned with the following metals: gold foil (99.99%), iron foil (99.9%), molybdenum foil (0.25 mm, 99.5%), and tungsten bar (ø 1.5 mm, 99.8%).

The X-ray photoelectron spectra were recorded on an Axis Ultra DLD spectrometer (Kratos) using monochromatic Al K_α radiation at an X-ray gun power of 150 W. The full spectra were registered with a step of 1 eV, the high-resolution spectra were recorded with a step of 0.1 eV. The preliminary calibration of the spectrometer energy scale corresponded to the following values of the peaks of standard samples (metal surfaces purified by ion sputtering): 83.96 eV for Au $4f_{7/2}$, 932.62 eV for Cu $2p_{3/2}$, and 368.21 eV for Ag $3d_{5/2}$. To eliminate the effect of sample charging, the spectra were recorded using a neutralizer. The spectra were referenced to the C–C/C–H state identified in the C 1s spectrum, to which an energy of 285.0 eV was assigned. The background of inelastic electron energy losses was subtracted using the Shirley method.

The surface morphology of the resulting nanocomposites was studied by scanning electron microscopy on a Hitachi TM4000Plus microscope (Japan) at an accelerating voltage of 15 kV in the secondary electron mode. The energy dispersive X-ray studies were carried out using a Bruker QUANTAX 75 spectrometer (Germany). The metal nanoparticles were analyzed by transmission electron microscopy using a LEO 912AB OMEGA instrument (Zeiss, Germany) at an accelerating voltage of 100 kV.

To evaluate the antibacterial activity of AuAc and FeAc, agar disk diffusion assays were performed using a gram-negative strain of *Escherichia coli* (ATCC 25922^{TM}) and a

gram-positive strain of *Bacillus cereus* (ATCC 11778^{TM}). For the experiments, a bacterial suspension (50 μL, 1×106 CFU/mL) was inoculated onto nutrient agar Petri dishes. Then the nanoparticle samples (200 μg) were applied to the plates. The samples were applied to sterile paper discs 6 mm in diameter. The control was a buffer solution (20 μL) containing 20 IU of penicillin and 20 μg of streptomycin. The plates were incubated with the test samples for 24 h at 37 °C. Then the average diameter of the zones with inhibited bacterial growth were measured.

Syntheses

The Au, Fe, and AuFe nanoparticles were obtained by metal vapor synthesis [35, 36]. In a typical experiment, 0.2–0.4 g of metal and 120–140 mL of acetone were evaporated. The co-condensation of the metal and organic ligand vapors was carried out in a 5-L static quartz reactor. The metal vapors were generated under vacuum of 10^{-2} Pa by resistive heating of a molybdenum boat for Au evaporation and a tungsten bar for Fe and AuFe. Then the metal vapors were co-condensed with acetone on the reactor walls cooled with liquid nitrogen (see Scheme S1 in the ESI). The duration of the synthesis was 40–60 min. After its completion, the cooling was removed, and the co-condensate matrix was heated to room temperature. The metal organosol was siphoned *in situ* from the reactor into an evacuated flask, from which acetone was further distilled off, and the resulting metal blacks were examined.

Conclusions

The mono- and bimetallic particles of Au, Fe, and AuFe were obtained by metal vapor synthesis using acetone as the reaction medium. Their compositions, surface, and antibacterial properties were investigated.

Using XPS, EDX, and SEM methods, it was shown that the resulting nanoparticles contain a significant amount of hydrocarbon compounds. The TEM analysis demonstrated that the use of acetone as an organic reagent in metal vapor synthesis affords Au and Fe nanoparticles with average sizes of 5.3 nm and 1.8 nm, respectively. A comparative analysis of the C 1s and O 1s spectra for the bimetallic nanoparticles revealed the presence of fragments of organic compounds containing C–C/C–H, C–O/C–O–C, C=O/O–C–O, and metal–carbon bonds.

The antibacterial activity was manifested by both of the monometal samples. Gold exhibited an inhibitory effect on gram-negative bacteria, while iron affected both gram-negative and gram-positive bacteria.

The results obtained demonstrate the prospects of further application of environmentally friendly metal vapor synthesis for the production of nanoparticles of biologically active metals.

Acknowledgements

This work was supported by the Russian Foundation for Basic Research (project no. 20-53-18006).

The XPS studies were carried out using the equipment of the Center for Molecular Composition Studies of INEOS RAS with financial support from the Ministry of Science and Higher Education of the Russian Federation (agreement no. 075-03-2023-642).

The authors are grateful to T. Batsalova for biological studies.

Corresponding author

* E-mail: alexandervasilkov@yandex.ru (A. Yu. Vasil'kov)

Electronic supplementary information

Electronic supplementary information (ESI) available online: SEM micrographs of the Au and Fe black nanoparticles, size distribution histograms of the Au and Fe nanoparticles, Au 4f photoelectron spectra of the AuAc and AuFeAc samples, scheme of the MVS setup. For ESI, see DOI: 10.32931/io2215a

References

1. M. P. Vinardell, M. Mitjans, *Nanomaterials*, **2015**, *5*, 1004–1021. DOI: 10.3390/nano5021004
2. G. Zhao, B. L. Rodriguez, *Int. J. Nanomed.*, **2013**, *8*, 61–71. DOI: 10.2147/IJN.S37859
3. M. J. Akhtar, H. A. Alhadlaq, S. Kumar, S. A. Alrokayan, M. Ahamed, *Arch. Toxicol*., **2015**, *89*, 1895–1907. DOI: 10.1007/s00204-015-1570-1
4. M. Z. Ahmad, S. Akhter, G. K. Jain, M. Rahman, S. A. Pathan, F. J. Ahmad, R. K. Khar, *Expert Opin. Drug Delivery*, **2010**, *7*, 927–942. DOI: 10.1517/17425247.2010.498473
5. W. Chen, W. Cai, L. Zhang, G. Wang, L. Zhang, *J. Colloid Interface Sci.*, **2001**, *238*, 291–295. DOI: 10.1006/jcis.2001.7525
6. R. Geethalakshmi, D. V. L. Sarada, *Int. J. Nanomed*., **2012**, *7*, 5375–5384. DOI: 10.2147/IJN.S36516
7. J. Turkevich, G. Kin, *Science*, **1970**, *169*, 873–879. DOI: 10.1126/science.169.3948.873
8. E. Attari, H. Nosrati, H. Danafar, H. K. Manjili, *J. Biomed. Mater. Res., Part A*, **2019**, *107*, 2492–2500. DOI: 10.1002/jbm.a.36755
9. M. Zamani, M. Rostami, M. Aghajanzadeh, H. K. Manjili, K. Rostamizadeh, H. Danafar, *J. Mater. Sci.*, **2018**, *53*, 1634–1645. DOI: 10.1007/s10853-017-1673-6
10. D. Seeburg, D. Liu, J. Radnik, H. Atia, M.-M. Pohl, M. Schneider, A. Martin, S. Wohlrab, *Catalysts*, **2018**, *8*, 42. DOI: 10.3390/catal8020042
11. A. V. Naumkin, A. V. Budnikov, M. I. Buzin, A. Yu. Vasil'kov, *INEOS OPEN*, **2021**, *4*, 232–236. DOI: 10.32931/io2126a
12. H. Cai, K. Li, J. Li, S. Wen, Q. Chen, M. Shen, L. Zheng, G. Zhang, X. Shi, *Small*, **2015**, *11*, 4584–4593. DOI: 10.1002/smll.201500856
13. P. Guardia, S. Nitti, M. E. Materia, G. Pugliese, N. Yaacoub, J.-M. Greneche, C. Lefevre, L. Manna, T. Pellegrino, *J. Mater. Chem. B*, **2017**, *5*, 4587–4594. DOI: 10.1039/C7TB00968B
14. A. Tomitaka, S. Ota, K. Nishimoto, H. Arami, Y. Takemura, M. Nair, *Nanoscale*, **2019**, *11*, 6489–6496. DOI: 10.1039/C9NR00242A
15. A. Majouga, M. Sokolsky-Papkov, A. Kuznetsov, D. Lebedev, M. Efremova, E. Beloglazkina, P. Rudakovskaya, M. Veselov, N. Zyk, Yu. Golovin, N. Klyachko, A. Kabanov, *Colloids Surf.*, *B*, **2015**, *125*, 104–109. DOI: 10.1016/j.colsurfb.2014.11.012
16. T. Kinoshita, S. Seino, K. Okitsu, T. Nakayama, T. Nakagawa, T. A. Yamamoto, *J. Alloys Compd.*, **2003**, *359*, 46–50. DOI: 10.1016/S0925-8388(03)00198-1
17. J. Lin, W. Zhou, A. Kumbhar, J. Wiemann, J. Fang, E. E. Carpenter, C. J. O'Connor, *J. Solid State Chem.*, **2001**, *159*, 26–31. DOI: 10.1006/jssc.2001.9117

18. J. C. Love, L. A. Estroff, J. K. Kriebel, R. G. Nuzzo, G. M. Whitesides, *Chem. Rev*., **2005**, *105*, 1103–1170. DOI: 10.1021/cr0300789
19. H. Zeng, X.-W. Du, S. C. Singh, S. A. Kulinich, S. Yang, J. He, W. Cai, *Adv. Funct. Mater*., **2012**, *22*, 1333–1353. DOI: 10.1002/adfm.201102295
20. J. L. Lyon, D. A. Fleming, M. B. Stone, P. Schiffer, M. E. Williams, *Nano Lett*., **2004**, *4*, 719–723. DOI: 10.1021/nl035253f
21. A. Yu. Vasil'kov, R. I. Dovnar, S. M. Smotryn, N. N. Iaskevich, A. V. Naumkin, *Antibiotics*, **2018**, *7*, 80. DOI: 10.3390/antibiotics7030080
22. K. A. Abd-Elsalam, M. A. Alghuthaymi, A. Shami, M. S. Rubina, S. S. Abramchuk, E. V. Shtykova, A. Yu. Vasil'kov, *J. Fungi*, **2020**, *6*, 112. DOI: 10.3390/jof6030112
23. G. Cárdenas-Triviño, C. Cruzat-Contreras, *J. Cluster Sci.*, **2018**, *29*, 1081–1088. DOI: 10.1007/s10876-018-1419-x
24. A. Vasil'kov, M. Rubina, A. Naumkin, M. Buzin, P. Dorovatovskii, G. Peters, Ya. Zubavichus, *Gels*, **2021**, *7*, 82. DOI: 10.3390/gels7030082
25. G. Cárdenas, V. Sáez, C. Cruzat, *J. Cluster Sci.*, **2017**, *28*, 1127–1144. DOI: 10.1007/s10876-016-1071-2
26. R. S. del Río, G. Cárdenas, *J. Cryst. Growth*, **2008**, *310*, 495–500. DOI: 10.1016/j.jcrysgro.2007.10.057
27. S. Amsarajan, B. R. Jagirdar, *Eur. J. Inorg. Chem.*, **2019**, 1374–1383. DOI: 10.1002/ejic.201801326
28. S. T. Lin, M. T. Franklin, K. J. Klabunde, *Langmuir*, **1986**, *2*, 259–260. DOI: 10.1021/la00068a027
29. D. Barbaro, L. Di Bari, V. Gandin, C. Evangelisti, G. Vitulli, E. Schiavi, C. Marzano, A. M. Ferretti, P. Salvadori, *PLoS One*, **2015**, *10*, e0123159. DOI: 10.1371/journal.pone.0123159
30. S. C. Davis, K. J. Klabunde, *J. Am. Chem. Soc.*, **1978**, *100*, 5973–5974. DOI: 10.1021/Ja00486A076
31. S. C. Davis, S. J. Severson, K. J. Klabunde, *J. Am. Chem. Soc.*, **1981**, *103*, 3024–3029. DOI: 10.1021/Ja00401A019
32. D. M. Gruen, D. H. W. Carstens, *J. Chem. Phys*., **1971**, *54*, 5206–5214. DOI: 10.1063/1.1674816
33. D. M. Mann, H. P. Broida, *J. Chem. Phys*., **1971**, *55*, 84–94. DOI: 10.1063/1.1675564
34. K. J. Klabunde, S. C. Davis, H. Hattori, Y. Tanaka, *J. Catal.*, **1978**, *54*, 254–268. DOI: 10.1016/0021-9517(78)90048-9
35. A. Vasil'kov, T. Batsalova, B. Dzhambazov, A. Naumkin, *Surf. Interface Anal.*, **2022**, *54*, 189–202. DOI: 10.1002/sia.7038
36. A. Yu. Vasil'kov, D. A. Migulin, V. M. Muzalevskiy, A. V. Naumkin, A. Yu. Pereyaslavtsev, Ya. V. Zubavichus, V. G. Nenajdenko, A. M. Muzafarov, *Mendeleev Commun*., **2022**, *32*, 478–481. DOI: 10.1016/j.mencom.2022.07.016
37. G. Beamson, D. Briggs, High Resolution XPS of Organic Polymers: The Scienta ESCA300 Database, Wiley, Chichester, New York, **1992**.